

Automatic multi-objective based feature selection for classification

Zhiguo Zhou¹, Shulong Li², Genggeng Qin², Michael Folkert¹, Steve Jiang¹, and Jing Wang^{1,*}

¹Medical Artificial Intelligence and Automation Laboratory (MAIA Lab), UT Southwestern Medical Center, Dallas, TX

²School of Biomedical Engineering, Southern Medical University, Guangzhou, China

Abstract: Accurately classifying the malignancy of lesions detected in a screening scan is critical for reducing false positives. Radiomics holds great potential to differentiate malignant from benign tumors by extracting and analyzing a large number of quantitative image features. Since not all radiomic features contribute to an effective classifying model, selecting an optimal feature subset is critical. This work proposes a new multi-objective based feature selection (MO-FS) algorithm that considers sensitivity and specificity simultaneously as the objective functions during feature selection. For MO-FS, we developed a modified entropy based termination criterion (METC) that stops the algorithm automatically rather than relying on a preset number of generations. We also designed a solution selection methodology for multi-objective learning that uses the evidential reasoning approach (SMOLER) to automatically select the optimal solution from the Pareto-optimal set. Furthermore, we developed an adaptive mutation operation to generate the mutation probability in MO-FS automatically. We evaluated the MO-FS for classifying lung nodule malignancy in low-dose CT and breast lesion malignancy in digital breast tomosynthesis. The experimental results demonstrated that the feature set selected by MO-FS achieved better classification performance than features selected by other commonly used methods.

Keywords: Malignancy classification; Radiomics; Feature selection; Multi-objective evolutionary algorithm; Evidential reasoning

1. Introduction

Accurately classifying the malignancy of lesions detected in a screening test is critical for reducing false positives and unnecessary follow-up tests. Several studies have shown that computer-aided diagnosis schemes can efficiently assist radiologists in differentiating malignant from benign tumors (Acharya et al., 2011; Verma et al., 2010; Wei et al., 2005). In recent years, radiomics has shown great potential for classifying lesion malignancy by extracting and analyzing a large number of quantitative imaging features (Aerts et al., 2014; Lambin et al., 2017). For example, radiomics has been successfully applied to lung nodule classification (Cirujeda et al., 2016; Ma et al., 2016) and breast lesion malignancy

* Jing Wang is the corresponding author. E-mail: Jing.Wang@UTSouthwestern.edu.

classification (Li et al., 2016; Valdora et al., 2018). In radiomics, typically several hundred features are extracted from segmented lesions (Aerts et al., 2014). However, not all of these features are discriminative, and many are correlated, redundant, or even irrelevant, which may reduce the model's performance. In addition, a high-dimensional feature space increases the model's complexity and may cause over-fitting.

Selecting a subset of relevant features from the original feature set (i.e., feature selection) is a critical step in radiomics model construction, as it can simplify the predictive model, increase the model's performance, reduce the dimensionality of the feature space, and speed up the learning processing (Xue et al., 2016). Current feature selection algorithms can be divided into two categories: filter approaches and wrapper approaches. Filter approaches use a suitable ranking criterion to score features and remove those that fall below a certain threshold (Chandrashekar and Sahin, 2014). Several filter approaches have been used for radiomic feature selection, including correlation coefficient analysis (CCA), mutual information maximization (MIM), minimum redundancy maximum relevance (mRMR), and relevance in estimating features (RELIEF) (Parmar et al., 2015). Filter approaches can be used as an initial step to remove redundant features, while wrapper approaches can further select features by evaluating the predictive performance of classifiers using the selected feature set. Sequential forward selection (SFS) (Chandrashekar and Sahin, 2014) and sequential backward selection (SBS) (Chandrashekar and Sahin, 2014) are the two classic wrapper algorithms. The evolutionary computation (EC) based feature selection method has also gained much attention and shown some success in recent years (Xue et al., 2016).

Because predictive model performance is evaluated in wrapper based feature selection approaches, evaluation criteria play an important role in selecting an appropriate feature set. Accuracy or area under the curve (AUC) has been used widely for evaluating model performance. However, a single metric may not suffice, especially for imbalanced positive and negative cases, as both sensitivity and specificity are required for a diagnostic procedure or modality (García-Nieto et al., 2009; Zhao, 2007; Zhou et al., 2017). Therefore, in this work, we consider feature selection as a multi-objective problem and use evolutionary computation for multi-objective optimization. Several multi-objective evolutionary algorithm based feature selection methods have been proposed, including genetic algorithm based methods (Emmanouilidis et al., 2000; Oliveira et al., 2002), particle swarm optimization based methods (Xue et al., 2013; Zhang et al., 2014), and a colony optimization based method (Vieira et al., 2009). However, these algorithms do not consider two issues. First, the number of generations that the multi-objective evolutionary algorithm runs is fixed arbitrarily. If this number is not large enough, we may only get local optimal solutions, and it may get stuck in a part of the Pareto-optimal solution set (Saxena et al., 2016). Second, the optimal solution is selected manually from the Pareto-optimal solution set. Since the

Pareto-optimal solution set always contains too many solutions, it is difficult for the decision maker to select the preferred solution (Zio and Bazzo, 2012).

To overcome these issues, we propose a new multi-objective based feature selection (MO-FS) algorithm in this work. The improvements of MO-FS include: 1) a modified entropy based termination criterion (METC) that stops the algorithm automatically rather than relying on a preset fixed number of generations; 2) a selection methodology for multi-objective learning using the evidential reasoning approach (SMOLER) that selects the optimal solution from the Pareto-optimal set automatically; and 3) an adaptive mutation operation designed to calculate mutation probability automatically instead of using a manually preset mutation probability.

In the proposed MO-FS, METC was developed based on an entropy based termination criterion for multi-objective evolutionary computation (Saxena et al., 2016). In addition to measuring the dissimilarities between the objective functions through relative entropy, as measured in the entropy based termination criterion, METC measures the dissimilarities for the selected feature set to select the most stable radiomic features. In SMOLER, the optimal solution selection rules are designed first and then combined using the evidential reasoning approach, which was originally proposed to deal with multiple attribute decision analysis problems (Yang and Singh, 1994; Yang and Xu, 2002; Zhou et al., 2013). In the adaptive mutation operation, the mutation probability is determined by correlation coefficients among individuals in one solution so that non-redundant features are selected with high probability. We evaluated the performance of MO-FS in two datasets: lung nodule malignancy classification in computed tomography (CT) (Armato et al., 2011) and breast lesion malignancy classification in digital breast tomosynthesis.

2. Methods

2.1. General description

The MO-FS framework for feature selection is shown in Figure 1. Before beginning the procedure, features are extracted from segmented images. MO-FS consists of two phases: (1) generating the Pareto-optimal solution set; and (2) selecting the best solution through SMOLER. Then, the discriminative features are selected.

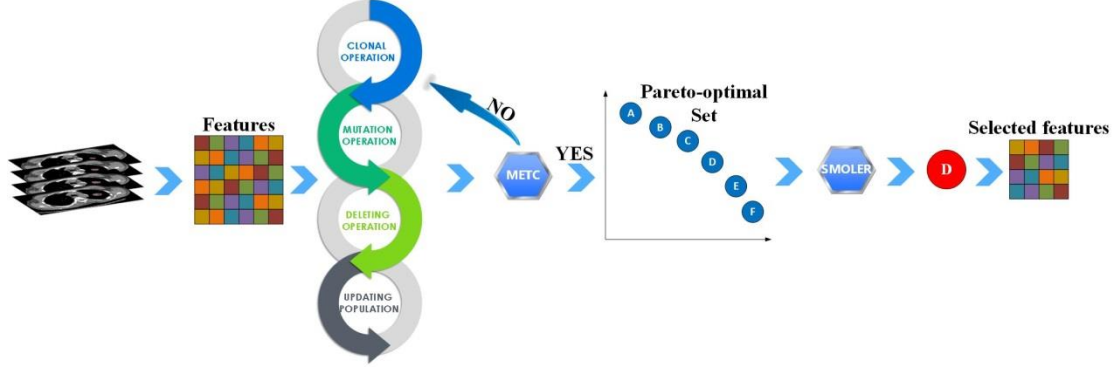


Figure 1: MO-FS Framework for feature selection.

When generating the Pareto-optimal solution set in the first phase, sensitivity and specificity are considered simultaneously as the objective functions. This phase consists of six steps, as follows: Step 1: Initialization. All solutions in the population are generated randomly and are denoted by $S(j) = \{s_1, \dots, s_P\}, j = 0$, where P is the population size and j is the generation number. Each solution is denoted by $s_p = \{I_p^1, \dots, I_p^N\}$, where N is the number of individuals (features). Binary coding is adopted for each solution in the population. In detail, “1” means the selected individual, while “0” means the unselected individual. The second step is the clonal operation. The proportional cloning strategy (Gong et al., 2008) is used, and the obtained cloned population $C(j)$ is generated. Step 3: Adaptive mutation operation. The mutation probability MP is generated automatically in this step, and the mutated solution set $M(j)$ is generated based on $C(j)$. Then, the new solution set $F(j)$, which combines $S(j)$ and $M(j)$, is generated. Step 4: Deleting operation. When $F(j)$ yields multiple same solutions, only the solution with the highest AUC is kept, and the remaining solutions constitute the new solution set $DF(j)$. When $\text{size}(DF(j)) < P$, the algorithm returns to step 2; otherwise, it continues to step 5. Step 5: Updating solution set. AUC based non-dominated sorting (Zhou et al., 2017) is used to update the solution set, and $UD(j)$ is generated. Step 6: Termination detection. If the solution set $UD(j)$ satisfies the METC, phase 1 ends; otherwise, let $j = j + 1$, $S(j) = UD(j)$, and the algorithm returns to step 2.

The second phase is divided into three steps. First, the Pareto front set (PD) is extracted from $UD(j)$. Then, the best solution D^* is selected from PD through SMOLER. Finally, the corresponding selected feature set SF is obtained.

The following sections describe the adaptive mutation operation, modified entropy based termination criterion, and SMOLER in detail.

2.2. Adaptive mutation operation

In the adaptive mutation operation, the mutation probability is set automatically based on correlation coefficients among features. First, the correlation coefficient matrix R is calculated as (Kendall et al., 1948):

$$R = \begin{bmatrix} |r_{1,1}| & \cdots & |r_{1,n}| \\ \vdots & \ddots & \vdots \\ |r_{n,1}| & \cdots & |r_{n,n}| \end{bmatrix}, \quad (1)$$

where $r_{i,j}$ represents the correlation coefficient between two features. Assume that there are K selected features in a solution s_p . Then, correlation coefficients denoted by $\{r_{i,1}, \dots, r_{i,K}\}$ between any individual feature I_p^i and K selected features can be extracted from R . If I_p^i is a selected feature, then the mutation probability of this feature is calculated as:

$$MP_i = \frac{\sum_{k=1, k \neq i}^K r_{i,k}}{K}. \quad (2)$$

If I_p^i is not selected in s_p , then,

$$MP_i = 1 - \frac{\sum_{k=1, k \neq i}^K r_{i,k}}{K}. \quad (3)$$

The above formulation for calculating mutation probability MP_i for feature I_p^i is based on the idea that, if the selected feature I_p^i is highly correlated with other selected features, then a higher mutation probability is calculated according to equation (2), so this feature has a higher chance to mutate and is unselected. On the other hand, if an unselected feature is highly correlated with other selected features, then a lower mutation probability for this unselected feature is calculated according to equation (3), so this feature has a lower chance to mutate and remains unselected. A random mutation RP_i is generated. If $MP_i > RP_i$, the mutation will perform; otherwise, the algorithm continues to the next individual.

2.3. Modified entropy based termination criterion (METC)

2.3.1. Entropy based termination criterion

Entropy based termination criterion (Saxena et al., 2016) consists of four stages: (1) generating a cell identification number for each solution; (2) obtaining the probability distribution for objective functions; (3) measuring the dissimilarity; and (4) detecting termination.

In the first stage, the solutions in the population are mapped into the range $[0, 1]$ through:

$$\bar{s}_j = \frac{s_j - O_{min,j}}{O_{max,j} - O_{min,j}}, \text{ for } j = 1, \dots, M, \quad (4)$$

where $O_{min,j}$ and $O_{max,j}$ define the minimum and maximum values, respectively, for the j th objective, and M is the objective number. Let n_b denote a fixed number of intervals, which is defined as an anchor point and bin width for each dimension. Assume that a vector $B = \{(\frac{0}{n_b}), (\frac{1}{n_b}), \dots, (\frac{n_b}{n_b})\}$ with size $n_b + 1$ defines a set of intervals, which satisfies $B_{k_j} \leq \bar{s}_j \leq B_{k_j+1}, k_j \in [0, \dots, n_b - 1]$. The cell identification number can be calculated as:

$$c = \sum_{j=1}^M k_j \times n_b^{j-1}. \quad (5)$$

Based on the cell identification number, the multi-dimensional histogram is generated in the second stage. Assume that there are $N = \{N_1, \dots, N_{n_b \times n_b}\}$ numbers in each bin. The probability distribution P for the current population is calculated as:

$$p_i = \frac{N_i}{\hat{N}}, i = 1, \dots, n_b \times n_b, \quad (6)$$

where \hat{N} represents the population size. Assume that $Q = \{q_1, \dots, q_{n_b \times n_b}\}$ is the probability distribution in the next generation. The dissimilarity between P and Q can be calculated in the third stage based on different situations.

1) For intersection set ($p_i \neq 0$ and $q_i \neq 0$):

$$D(p, q)_I = KL(p|q) + KL(q|p), \quad (7)$$

where,

$$KL(p|q) = -\sum \frac{p(x_i)}{2} \log \left\{ \frac{q(x_i)}{p(x_i)} \right\}, \quad KL(q|p) = -\sum \frac{q(x_i)}{2} \log \left\{ \frac{p(x_i)}{q(x_i)} \right\}. \quad (8)$$

2) For non-interaction set ($p_i = 0$ or $q_i = 0$):

$$D(p, q)_y = D(p, q)_{y_p} + D(p, q)_{y_q}, \quad (9)$$

where,

$$D(p, q)_{y_p} = -\sum \frac{p(x_i)}{2} \log \{p(x_i)\}, \quad D(p, q)_{y_q} = -\sum \frac{q(x_i)}{2} \log \{q(x_i)\}. \quad (10)$$

Therefore, the final dissimilarity $D_o(p, q)$ between generations is:

$$D_O(p, q) = D(p, q)_I + D(p, q)_y. \quad (11)$$

Finally, the generation counter is denoted by t , and the current generation is denoted by i . D_i represents the $D_O(p, q)$ in the i th generation, and M_t and S_t are the mean and standard deviation of $D_O(p, q)$ from the first to the i th generation, calculated as:

$$M_1 = D_1 \text{ and } M_t = \frac{1}{t} \sum_{i=1}^t D_i, \text{ where } t \geq 2, \quad (12)$$

$$S_t = \frac{1}{t} \sum_{i=1}^t (D_i - M_t)^2. \quad (13)$$

When M_t and S_t in a manually defined number (n_s) of successive generations coincide up to a pre-specified number of decimal (n_p), the algorithm will be terminated.

2.3.2. Proposed METC

In addition to considering the dissimilarity of objective function values between successive generations, our modified entropy termination criterion (METC) also considers the dissimilarity of the selected features between generations to obtain more stable features. The METC workflow is summarized in Algorithm 1. After generating the cell identification number through objective functions, the selected features for each solution in each cell are also obtained. As with the entropy based termination criterion, it is assumed that there are $N = \{N_1, \dots, N_{n_b \times n_b}\}$ (n_b is the number of intervals) numbers in each bin for population P . For each bin $B_i, i = 1, \dots, n_b \times n_b$, the selected features in each solution are denoted by $F_i^{B_i, P} = \{F_1^{B_i, P}, \dots, F_{N_i}^{B_i, P}\}, i = 1, \dots, n_b \times n_b$, where $F_i^{B_i, P}$ is a binary vector. Hence, the probability distribution for selected features in each bin is calculated as:

$$p_{B_i}^P = \frac{\sum_{j=1}^{N_i} F_j^{B_i, P}}{N_i \times N}, i = 1, \dots, n_b \times n_b, \quad (14)$$

where N is the feature number and j represents the number in each bin. Similarly, we can obtain $p_{B_i}^Q$ for the next generation Q . Then, the dissimilarity of the selected features $D_{B_i}(p, q)$ for each bin between P and Q can be calculated through equations (7)-(11), and the final dissimilarity $D(p, q)$ is:

$$D(p, q) = D_O(p, q) + \sum_{i=1}^{n_b \times n_b} D_{B_i}(p, q). \quad (15)$$

Algorithm 1: METC

Input: Multiple successive generations

Step 1: Generating cell identification number. The unique cell identification number for all solutions in each generation is calculated through Eq. (5).

Step 2: Obtaining probability distribution. The probability distribution for the objective functions is calculated through Eq. (7), while the probability distribution for selected features in each bin is calculated through Eq. (15).

Step 3: Measuring dissimilarity. $D_O(p, q)$ and $D_{B_i}(p, q)$ are calculated first, then $D(p, q)$ is calculated through Eq. (16).

Output: Detecting termination. When M_t and S_t coincide up to a pre-specified number of decimal places, the algorithm terminates.

An example of calculating $D_{B_i}(p, q)$ will help illustrate the feature based dissimilarity calculation in the METC. Assume that there are 4 cells, the population size is 9, and the feature number is 10. Figure 2 shows the assignment of the unique cell identification number to each cell for two generations. Tables 1 and 2 show the corresponding selected results for each solution in two generations. For cell 2 in generation 1 (Fig. 2(a)), the selected feature histogram is generated based on solutions 1 and 2. Similarly, the selected feature histogram for cell 2 in generation 2 can also be obtained (Fig. 2(b)). Then, the probability distribution for each generation can be obtained:

$$p_{B_2}^1 = \left\{ \frac{1}{10}, \frac{1}{20}, 0, \frac{1}{20}, 0, \frac{1}{10}, \frac{1}{20}, \frac{1}{10}, \frac{1}{20}, 0 \right\}, \quad (16)$$

$$p_{B_2}^2 = \left\{ \frac{1}{20}, \frac{3}{40}, \frac{1}{20}, \frac{3}{40}, \frac{1}{20}, \frac{1}{20}, \frac{1}{20}, \frac{3}{40}, \frac{1}{20}, \frac{1}{20} \right\}. \quad (17)$$

The dissimilarity can be calculated according to equations (7)-(11):

$$D_{B_2}(p_{B_2}^1, p_{B_2}^2) = 0.2731. \quad (18)$$

The dissimilarities for another three bins can be calculated in the same way. After summing them, the final dissimilarity is,

$$D(p_{B_2}^1, p_{B_2}^2) = 1.5406. \quad (19)$$

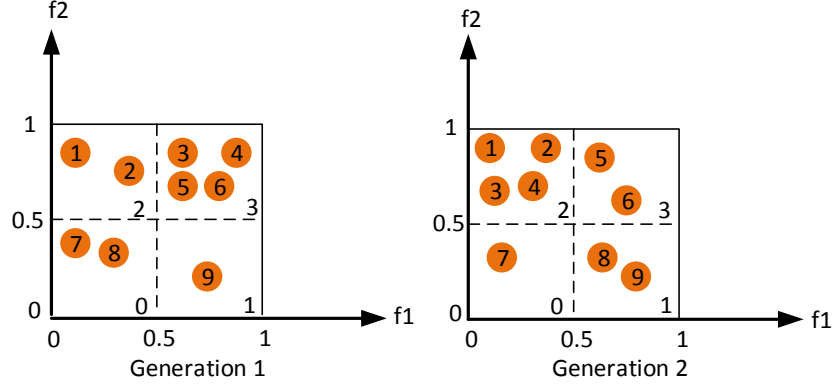


Figure 2: Assignment of the unique cell identification for each cell in two generations. The orange circles are the solutions, and 0-3 inside the cells represents the cell numbers.

Table 1: Selected results for solutions in generation 1.

solution	Selected results									
1	1	1	0	0	0	1	1	1	1	0
2	1	0	0	1	0	1	0	1	0	0
3	0	1	1	0	1	0	1	1	1	0
4	1	1	1	0	0	0	1	0	1	1
5	1	0	1	1	0	1	0	0	1	1
6	0	1	1	0	1	0	0	0	0	1
7	1	0	0	0	1	1	1	0	0	0
8	0	1	1	0	0	1	1	0	1	1
9	1	1	0	1	1	0	0	1	1	0

Table 2: Selected results for solutions in generation 2.

solution	Selected results									
1	0	1	1	0	0	0	1	1	1	0
2	1	1	0	1	1	1	0	1	0	1
3	1	0	0	1	1	0	1	1	1	0
4	0	1	1	1	0	1	0	0	0	1
5	1	1	0	1	1	0	1	1	0	1
6	0	0	1	1	1	0	1	0	1	0
7	1	1	0	1	0	1	1	0	1	0
8	0	0	1	1	0	1	0	1	1	1
9	0	1	1	0	1	1	0	1	1	0

2.4. Solution selection methodology for multi-objective learning using the evidential reasoning approach (SMOLER)

The procedures of SMOLER are shown in Algorithm 2. Assume that there are M_1 objective functions and K solutions $P = \{P_1, P_2, \dots, P_K\}$ in the Pareto solution set. To select the optimal solution, several decision rules need to be set. These rules include two types: one type is based on the objective function denoted by F_1 , and the other type is based on the preference and prior knowledge denoted by F_2 . Therefore, two objective functions (sensitivity and specificity) are taken as the first two rules, and the F_1 is,

$$F_1^k = \{f_{sen}^k, f_{spe}^k\}, k = 1, 2, \dots, K. \quad (20)$$

Area under the curve (AUC), an important evaluation criterion to determine whether the model is reliable, is adopted as the first rule in F_2 . In addition, to select a solution with balanced sensitivity and specificity, the relative distance is defined to evaluate the solution, that is,

$$f_{RD}^k = |f_{sen}^k - f_{spe}^k|^2, k = 1, 2, \dots, K. \quad (21)$$

So F_2 is,

$$F_2^k = \{f_{AUC}^k, f_{RD}^k\}, k = 1, 2, \dots, K. \quad (22)$$

When combining F_1 and F_2 , the final rule set F is,

$$F = \{f_1^k, f_2^k, f_3^k, f_4^k\}, k = 1, 2, \dots, K, \quad (23)$$

where $f_1^k = f_{sen}^k$, $f_2^k = f_{spe}^k$, $f_3^k = f_{AUC}^k$, and $f_4^k = f_{RD}^k$. Assume that there are N reference points for each rule in F , which are used to assess each solution for all rules (Yang, 2001), and the reference points are denoted by $H = \{H_1, H_2, \dots, H_N\}$. For the first three rules in F , the higher the values, the better the solutions. For the fourth rule, the solutions are better when the value is lower. Thus, the reference value $H_{i,j}$ for each rule i at reference point j is calculated as follows:

$$H_{i,j} = \begin{cases} \min(f_i^k) + (j-1) \times \frac{\max(f_i^k) - \min(f_i^k)}{N-1}, & i = 1, 2, 3 \\ \max(f_i^k) - (j-1) \times \frac{\max(f_i^k) - \min(f_i^k)}{N-1}, & i = 4 \end{cases}, \quad (24)$$

where $j = 1, 2, \dots, N, k = 1, 2, \dots, K$. The optimal solution selection can be modeled using the following expectations (Yang, 2001):

$$S(P_k) = \{H_{i,j}, \beta_{i,j}(P_k), j = 1, 2, \dots, N\}, i = 1, 2, \dots, M, k = 1, 2, \dots, K, \quad (25)$$

where $\beta_{i,j}(P_k) \geq 0$ and $\sum_{j=1}^N \beta_{i,j}(P_k) = 1$. $\beta_{i,j}(P_k)$ represents a degree of belief for solution P_k . Similar to the reference value $H_{i,j}$, $\beta_{i,j}(P_k)$ is calculated under the two situations (rules 1-3 and rule 4) in the third step. For rules 1-3, $\beta_{i,j}(P_k)$ is calculated as:

$$\beta_{i,j}(P_k) = \frac{H_{i,j+1} - f_i^k}{H_{i,j+1} - H_{i,j}}, \quad \beta_{i,j+1}(P_k) = 1 - \beta_{i,j}(P_k), \text{ when } H_{i,j} \leq f_i^k \leq H_{i,j+1}, \quad (26)$$

$$\beta_{i,p}(P_k) = 0 \quad p = 1, 2, \dots, N, \text{ and } p \neq j, j+1, i = 1, 2, 3.$$

For the fourth rule, $\beta_{i,j}(P_k)$ is calculated as :

$$\beta_{i,j}(P_k) = \frac{H_{i,j} - f_i^k}{H_{i,j} - H_{i,j+1}}, \beta_{i,j+1}(P_k) = 1 - \beta_{i,j}(P_k), \text{ when } H_{i,j+1} \leq f_i^k \leq H_{i,j}, \quad (27)$$

$$\beta_{i,p}(P_k) = 0 \quad p = 1, 2, \dots, N, \text{ and } p \neq j, j+1, i = 4.$$

The belief degrees for each rule can generate a belief degree matrix for all feasible solutions:

$$S_k = \begin{bmatrix} \beta_{1,1} & \beta_{1,2} & \cdots & \beta_{1,N} \\ \beta_{2,1} & \beta_{2,2} & \cdots & \beta_{2,N} \\ \beta_{3,1} & \beta_{3,2} & \cdots & \beta_{3,N} \\ \beta_{4,1} & \beta_{4,2} & \cdots & \beta_{4,N} \end{bmatrix}, k = 1, 2, \dots, K. \quad (28)$$

In the fourth step, all the rules in S_k are combined through the ER approach. Assume that the weights for each rule are denoted by $\omega_i, i = 1, \dots, 4$, which satisfies the following constraints:

$$0 \leq \omega_i \leq 1, \sum_{i=1}^M \omega_i = 1. \quad (29)$$

The final assessment $D(P_k)$ for solution P_k is represented by:

$$D(P_k) = \{(H_{k,j}, \beta_{k,j}), j = 1, 2, \dots, N\}, k = 1, 2, \dots, K. \quad (30)$$

Then, the belief degree $\beta_{k,j}$ for solution P_k at each reference point j in $D(P_k)$ is calculated using the evidential reasoning algorithm (Wang et al., 2006):

$$\beta_{k,j} = \frac{\mu \times [\prod_{i=1}^M (\omega_i \beta_{i,j}(P_k) + 1 - \omega_i \sum_{j=1}^N \beta_{i,j}(P_k)) - \prod_{i=1}^M (1 - \omega_i \sum_{j=1}^N \beta_{i,j}(P_k))]}{1 - \mu \times [\prod_{i=1}^M (1 - \omega_i)]}, \quad (31)$$

$$\mu = [\sum_{j=1}^N \prod_{i=1}^M (\omega_i \beta_{i,j}(P_k) + 1 - \omega_i \sum_{j=1}^N \beta_{i,j}(P_k)) - (N-1) \prod_{i=1}^M (1 - \omega_i \sum_{j=1}^N \beta_{i,j}(P_k))]^{-1}. \quad (32)$$

To select the optimal solution, the utility for $P_k, k = 1, 2, \dots, K$ is then calculated. Since there are N reference points, N evaluation grades are also needed. Assume that the utility of the grades $u(H_j)$ is equidistantly distributed in the utility space, i.e., $u(H_j) = \frac{j-1}{N-1}, j = 1, 2, \dots, N$. Then, the utility for P_k is calculated:

$$U(P_k) = \sum_{j=1}^N u_j \beta_{k,j}, k = 1, 2, \dots, K. \quad (33)$$

The final solution P^* is selected by:

$$U^* = \max(U(P_k), k = 1, 2, \dots, K). \quad (34)$$

Algorithm 2: SMOLER

Input: Pareto solution $P = \{P_1, P_2, \dots, P_K\}$, weight $\omega_i, i = 1, 2, \dots, M$, and number of reference points N .

Step 1: Generate solution selection rules $F^k, k = 1, 2, \dots, K$.

Step 2: Calculate reference values $H_{i,j}, i = 1, 2, \dots, M, j = 1, 2, \dots, N$.

Step 3: Calculate belief degrees $\beta_{i,j}(P_k), i = 1, 2, \dots, M, j = 1, 2, \dots, N, k = 1, 2, \dots, K$.

Step 4: Calculate utilities $U(P_k), k = 1, 2, \dots, K$.

Output: Select the final solution P^* .

3. Experiments and Discussion

3.1. Datasets

We first evaluated MO-FS using the Lung Image Database Consortium and Image Database Resource Initiative (LIDC-IDRI) dataset, which consists of 1,010 patients with thoracic computed tomography (CT) imaging and annotation results from four radiologists. In this dataset, 7,371 lesions were marked as nodules by at least one radiologist, and malignancy suspiciousness was rated on a scale of 1 to 5 (1 indicates the lowest malignancy suspiciousness, and 5 indicates the highest). This study considered nodules 3 mm or larger in size. We obtained the malignancy suspiciousness rate by averaging the suspicion level from the radiologists. After removing ambiguous nodules with an average suspicion level of 3, 431 malignant and 795 benign nodules remained. All nodules were contoured manually by radiologists. Typical malignant and benign nodules in this dataset are shown in Figure 3.

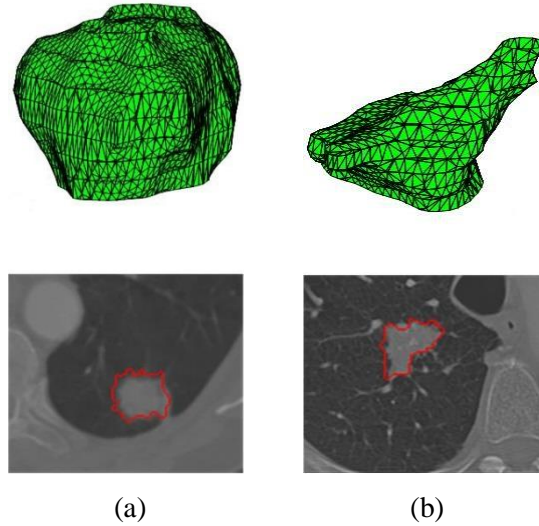


Figure 3: Benign (a) and malignant (b) lung nodules. The first row is the 3D tumor, and the second row is the corresponding 2D CT images.

We then evaluated MO-FS by classifying breast lesion malignance in a dataset of digital breast tomosynthesis (BLM-DBT). The patient DBT images comprise 278 malignant and 685 benign cases. Each lesion on DBT was initially contoured by one of eight radiologists with more than 3 years of experience in breast cancer diagnosis. Two additional radiologists with more than 5 years of experience reviewed and modified the contours if needed. The malignancy status was validated through biopsy.

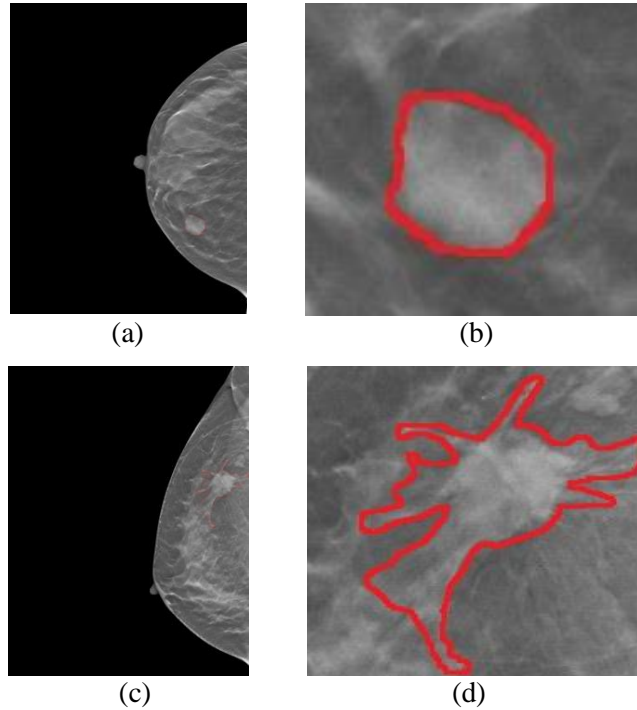


Figure 4: Benign and malignant breast tumors. (a) is the original image and (b) is the tumor region for a benign case. (c) is the original image and (d) is the tumor region for a malignant case.

3.2. Setup

Three types of radiomic features – intensity, texture, and geometry – and 257 features in total were extracted. The population size was set as 100 in MO-FS. In METC, the number of intervals n_b was set as 4, while both the number (n_s) of successive generations and the number of decimal (n_p) were set as 2. In SMOLER, the reference point number was set as 5. Among the four rules, sensitivity and specificity are the objective functions, so they are slightly more important than relative distance and AUC. Accordingly, the weight was set as $\omega = \{0.3, 0.3, 0.2, 0.2\}$. To demonstrate MO-FS’s performance, we compared it with five commonly used feature selection methods: correlation based feature selection (CFS) (Roffo et al., 2015), evolutionary computation based feature selection (ECFS) (Roffo et al., 2017), minimum redundancy maximum relevance (mRMR), relevance in estimating features (RELIEF), and sequential forward selection (SFS). We used support vector machine with radial basis function as a

training model for all feature selection methods and performed two-folder cross-validation. A trained model evaluated the performance through the selected feature set. Area under the curve (AUC), accuracy (ACC), sensitivity (SEN), and specificity (SPE) were used for quantitative evaluation. All methods were performed ten times. The mean and standard deviation for each evaluation criterion were calculated from 10 times results.

3.3. Results and analysis

Table 3 summarizes the model performance on the LIDC-IDRI dataset after being trained using the feature sets selected by six feature selection methods. The MO-FS obtained better ACC, AUC, and sensitivity than the other methods, while SFS achieved slightly higher specificity than MO-FS. MO-FS also obtained the smallest difference (0.0481) between sensitivity and specificity. Similar results were obtained in BLM-DBT as shown in Table 4. The proposed MO-FS outperforms the other methods for AUC, accuracy, and specificity, but not sensitivity. The sensitivity and specificity are more balanced as well in MO-FS. In both studies, MO-FS achieves the highest AUC and accuracy due to the reliability of the selected feature set.

Table 3: Feature selection performance for different methods in LIDC-IDRI. The best results are in bold.

Method	AUC	ACC	SEN	SPE
CFS	0.8987±0.0008	0.8469±0.0018	0.8018±0.0020	0.8714±0.0024
ECFS	0.9101±0.0008	0.8621±0.0016	0.8053±0.0023	0.8928±0.0026
mRMR	0.9061±0.0005	0.8512±0.0019	0.8039±0.0044	0.8769±0.0017
RELIEF	0.9125±0.0006	0.8653±0.0021	0.8037±0.0025	0.8986±0.0023
SFS	0.9055±0.0013	0.8649±0.0031	0.7527±0.0026	0.9258±0.0022
MO-FS	0.9349±0.0017	0.8899±0.0014	0.8587±0.0057	0.9068±0.0043

Table 4: Feature selection performance for different methods in BLM-DBT. The best results are in bold.

Method	AUC	ACC	SEN	SPE
CFS	0.7318±0.0008	0.6653±0.0010	0.6685±0.0162	0.6576±0.0133
ECFS	0.6830±0.0067	0.6423±0.0069	0.6349±0.0149	0.6604±0.0167
mRMR	0.7590±0.0044	0.7175±0.0040	0.7474±0.0048	0.6439±0.0085
RELIEF	0.7757±0.0024	0.7370±0.0052	0.7721±0.0077	0.6504±0.0079
SFS	0.7773±0.0030	0.7407±0.0035	0.8097±0.0068	0.5707±0.0142
MO-FS	0.8194±0.0043	0.7563±0.0051	0.7640±0.0020	0.7958±0.0028

Figure 5 shows the solutions generated, marked in blue, and the selected optimal solution, marked in red, for two running of the predictive model on LIDC-IDRI and BLM-DBT. The optimal solutions are

always located at the “knee” point, which fully considers the trade-off between the two objective functions.

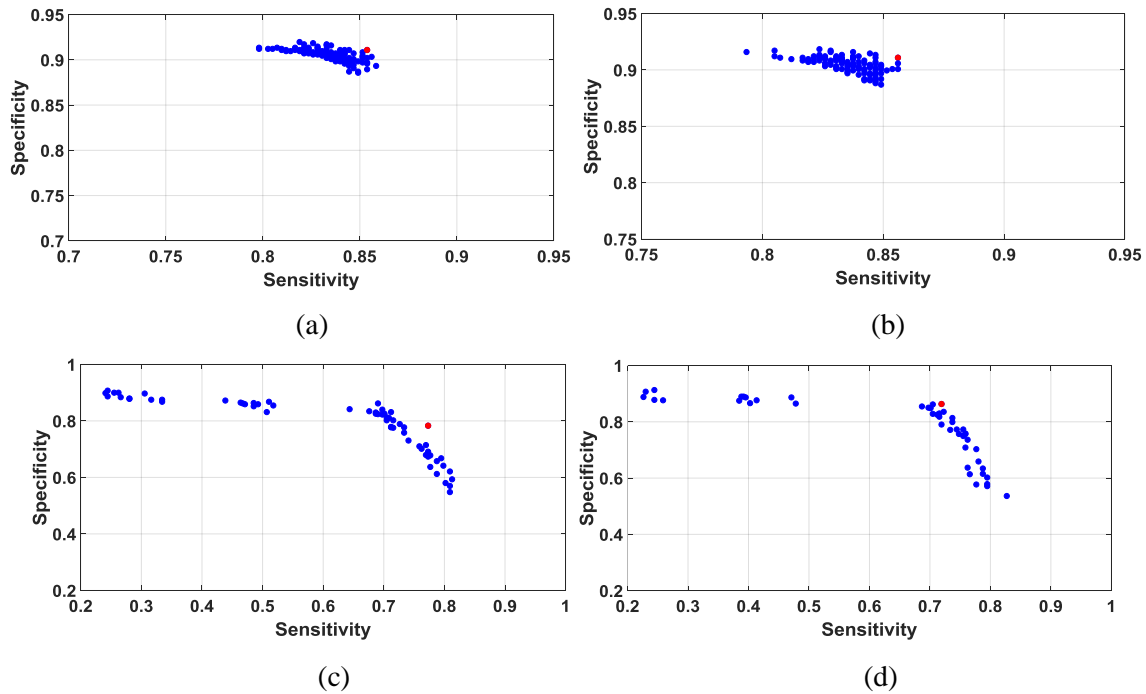


Figure 5: Generated solutions (blue labels) and selected optimal solution (red label) for LIDC-IDRI (a-b) and BLM-DBT (c-d).

Figure 6 shows the dissimilarity measure results for two running of the predictive model on the two datasets as the number of generation increases for the two datasets. With increasing of the generations, the dissimilarity measure results become smaller, showing the convergence of the algorithm. The proposed algorithm stopped automatically after a certain number of iterations, with different iterations for different datasets.

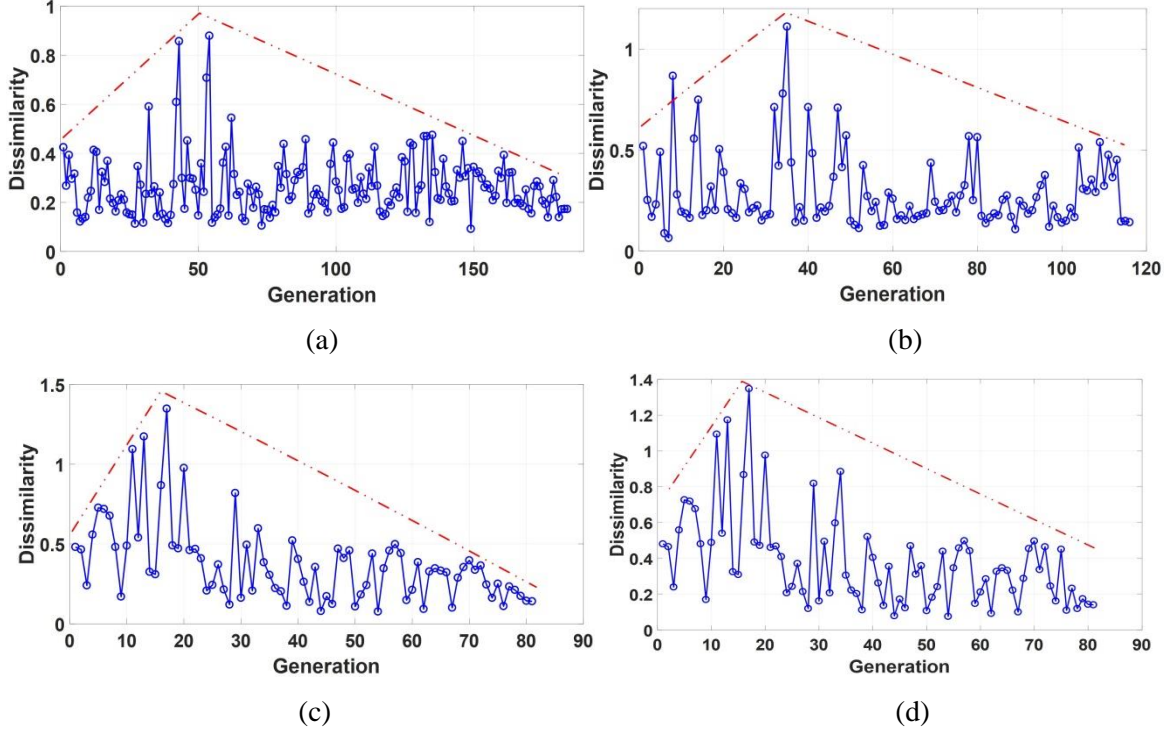


Figure 6: Dissimilarity measure results with the increasing number of generations for LIDC-IDRI (a-b) and BLM-DBT (c-d). Blue lines are the dissimilarity measure results, and red lines are the dissimilarity trends.

To illustrate how the termination detection criterion affects the stability of the selected features, Figure 7 shows the frequencies of the selected features in ten running of the predictive model on LIDC-IDRI and BLM-DBT. Compared with the entropy based termination criterion (ETC), METC selects the same features more frequently, showing better stability and repeatability.

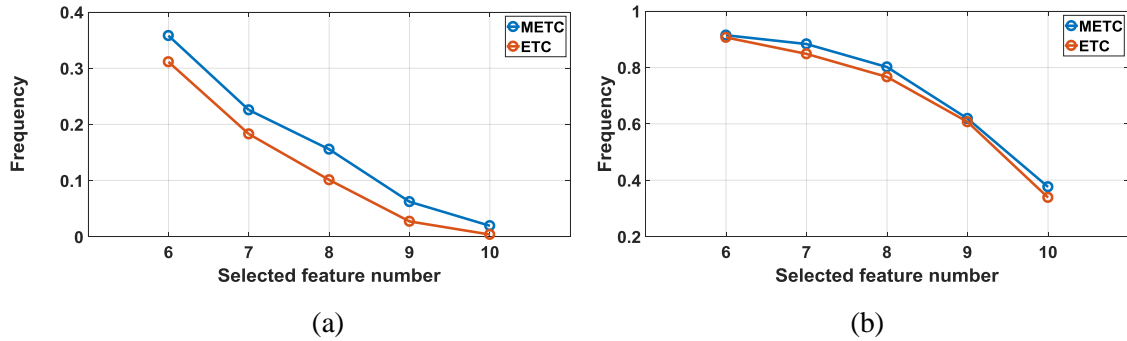


Figure 7: The frequency of the selected features for ETC and METC: (a) LIDC-IDRI and (b) BLM-DBT.

3.4. Sensitivity analysis of SMOLER

We investigated the influence of the weights and the reference number on the SMOLER selection results by analyzing the sensitivity. While analyzing the influence of the weight, the reference number r was set at 5. Assume that the four weights are denoted by $\{\omega_1, \omega_2, \omega_3, \omega_4\}$. We set $\omega_1 = \omega_2$ and $\omega_3 = \omega_4 = \frac{1-2\omega_1}{2}$, and ω_1 increased from 0.25 to 0.4 in steps of 0.05. When we analyzed the sensitivity of the reference number, r increased from 5 to 11 in steps of 1, and the weight was fixed at $\{0.3, 0.3, 0.2, 0.2\}$. The sensitivity analysis of the weights for the two datasets is shown in Figure 8. The first row shows two examples for LIDC-IDRI, and the second row shows results for BLM-DBT. The results from LIDC-IDRI changed slightly with different weights, but there was no change for BLM-DBT. The results from analyzing the reference number (Fig. 9) show that there were no changes for any results, except in Figure 9(a), which shows a slight change (of 0.01) with different reference numbers. These results demonstrate the robustness of SMOLER.

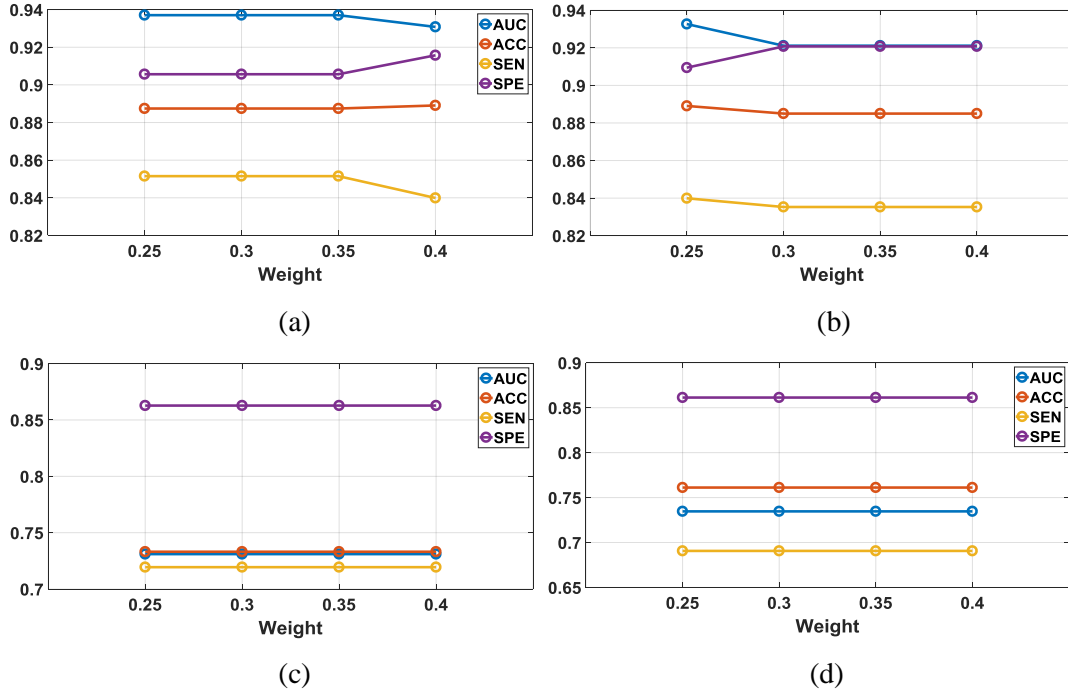


Figure 8: Sensitivity analysis for weight in two running of the predictive model. The x-axis represents the increasing of ω_1 . The first row is the results for LIDC-IDRI, and the second row is the results for BLM-DBT.

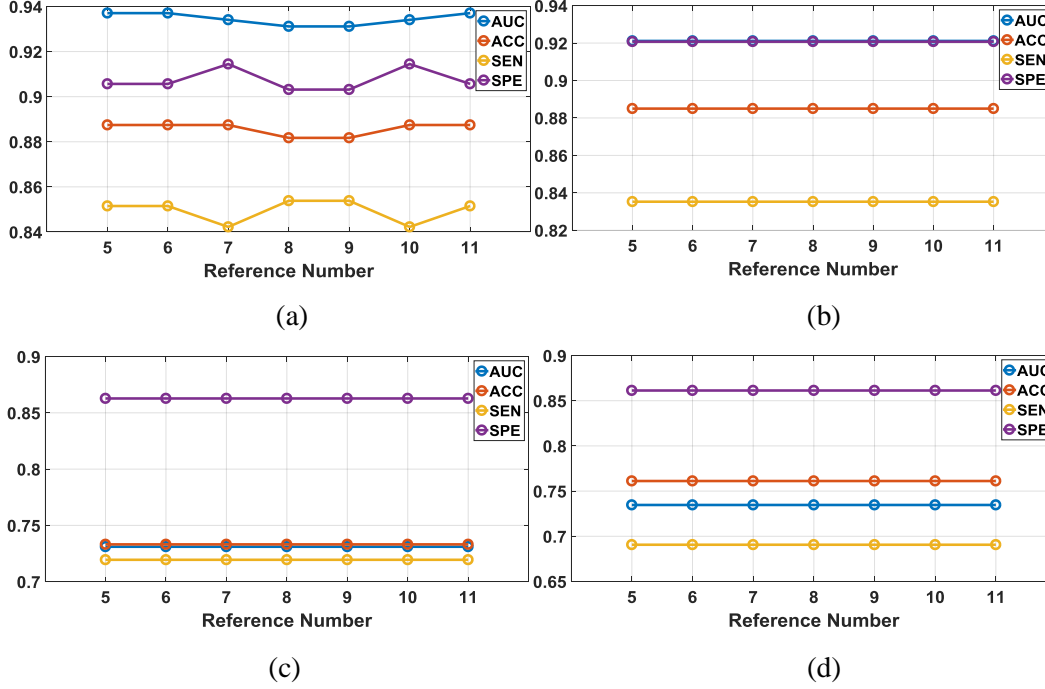


Figure 9: Sensitivity analysis for reference number in two running of the predictive model. The first row is the results for LIDC-IDRI, and the second row is the results for BLM-DBT.

4. Conclusions

This study proposed a multi-objective based feature selection (MO-FS) algorithm for selecting radiomic features for classification problems. In MO-FS, the algorithm's termination was detected automatically by a new modified entropy based termination criterion (METC) so that the generation does not need be set manually. The METC also showed better stability for the selected feature subset than ETC. To select the optimal feature subset automatically, we developed a solution selection methodology for multi-objective learning using the evidential reasoning approach (SMOLER). Furthermore, we designed an adaptive mutation operation, which generates mutation probability automatically. We used two datasets to evaluate the performance of the MO-FS and compared it to several well-known feature selection methods. The classification performance showed that MO-FS outperformed other methods in selecting a feature set.

In this work, we mainly focus on binary classification problems. Therefore, the MO-FS takes sensitivity and specificity as the objectives. However, for multi-class prediction problems, such as tumor staging, more objectives (more than three) need to be considered. Thus, a many-objective based algorithm (Ishibuchi et al., 2008) needs to be developed to handle multi-class prediction. As more objectives and

more rules are needed in SMOLER, manually setting the weights for different objectives becomes challenging, so a model for optimizing the weights is needed for SMOLER.

Acknowledgement

This work was supported in part by the American Cancer Society (ACS-IRG-02-196) and the US National Institutes of Health (5P30CA142543). The authors would like to thank Dr. Jonathan Feinberg for editing the manuscript.

Reference

- Acharya, U., Faust, O., Sree, S.V., Molinari, F., Garberoglio, R., Suri, J., 2011. Cost-effective and non-invasive automated benign & malignant thyroid lesion classification in 3D contrast-enhanced ultrasound using combination of wavelets and textures: a class of ThyroScan™ algorithms. *Technology in cancer research & treatment* 10, 371-380.
- Aerts, H.J., Velazquez, E.R., Leijenaar, R.T., Parmar, C., Grossmann, P., Cavalho, S., Bussink, J., Monshouwer, R., Haibe-Kains, B., Rietveld, D., 2014. Decoding tumour phenotype by noninvasive imaging using a quantitative radiomics approach. *Nature communications* 5.
- Armato, S.G., McLennan, G., Bidaut, L., McNitt - Gray, M.F., Meyer, C.R., Reeves, A.P., Zhao, B., Aberle, D.R., Henschke, C.I., Hoffman, E.A., 2011. The lung image database consortium (LIDC) and image database resource initiative (IDRI): a completed reference database of lung nodules on CT scans. *Medical physics* 38, 915-931.
- Chandrashekar, G., Sahin, F., 2014. A survey on feature selection methods. *Computers & Electrical Engineering* 40, 16-28.
- Cirujeda, P., Cid, Y.D., Müller, H., Rubin, D., Aguilera, T.A., Loo, B.W., Diehn, M., Binefa, X., Depeursinge, A., 2016. A 3-D Riesz-covariance texture model for prediction of nodule recurrence in lung CT. *IEEE transactions on medical imaging* 35, 2620-2630.
- Emmanouilidis, C., Hunter, A., MacIntyre, J., 2000. A multiobjective evolutionary setting for feature selection and a commonality-based crossover operator, *Evolutionary Computation*, 2000. Proceedings of the 2000 Congress on. IEEE, pp. 309-316.
- García-Nieto, J., Alba, E., Jourdan, L., Talbi, E., 2009. Sensitivity and specificity based multiobjective approach for feature selection: Application to cancer diagnosis. *Information Processing Letters* 109, 887-896.
- Gong, M., Jiao, L., Du, H., Bo, L., 2008. Multiobjective immune algorithm with nondominated neighbor-based selection. *Evolutionary Computation* 16, 225-255.
- Ishibuchi, H., Tsukamoto, N., Nojima, Y., 2008. Evolutionary many-objective optimization, *Genetic and Evolving Systems*, 2008. GEFS 2008. 3rd International Workshop on. IEEE, pp. 47-52.
- Kendall, M.G., Stuart, A., Ord, J.K., 1948. *The advanced theory of statistics*. JSTOR.
- Lambin, P., Leijenaar, R.T., Deist, T.M., Peerlings, J., de Jong, E.E., van Timmeren, J., Sanduleanu, S., Larue, R.T., Even, A.J., Jochems, A., 2017. Radiomics: the bridge between medical imaging and personalized medicine. *Nature Reviews Clinical Oncology*.
- Li, H., Zhu, Y., Burnside, E.S., Huang, E., Drukker, K., Hoadley, K.A., Fan, C., Conzen, S.D., Zuley, M., Net, J.M., 2016. Quantitative MRI radiomics in the prediction of molecular classifications of breast cancer subtypes in the TCGA/TCIA data set. *NPJ breast cancer* 2, 16012.

Ma, J., Wang, Q., Ren, Y., Hu, H., Zhao, J., 2016. Automatic lung nodule classification with radiomics approach, Medical Imaging 2016: PACS and Imaging Informatics: Next Generation and Innovations. International Society for Optics and Photonics, p. 978906.

Oliveira, L.S., Sabourin, R., Bortolozzi, F., Suen, C.Y., 2002. Feature selection using multi-objective genetic algorithms for handwritten digit recognition, Pattern Recognition, 2002. Proceedings. 16th International Conference on. IEEE, pp. 568-571.

Parmar, C., Grossmann, P., Bussink, J., Lambin, P., Aerts, H.J., 2015. Machine learning methods for quantitative radiomic biomarkers. Scientific reports 5.

Roffo, G., Melzi, S., Castellani, U., Vinciarelli, A., 2017. Infinite Latent Feature Selection: A Probabilistic Latent Graph-Based Ranking Approach. arXiv preprint arXiv:1707.07538.

Roffo, G., Melzi, S., Cristani, M., 2015. Infinite feature selection, Proceedings of the IEEE International Conference on Computer Vision, pp. 4202-4210.

Saxena, D.K., Sinha, A., Duro, J.A., Zhang, Q., 2016. Entropy-Based Termination Criterion for Multiobjective Evolutionary Algorithms. IEEE Transactions on Evolutionary Computation 20, 485-498.

Valdora, F., Houssami, N., Rossi, F., Calabrese, M., Tagliafico, A.S., 2018. Rapid review: radiomics and breast cancer. Breast cancer research and treatment, 1-13.

Verma, B., McLeod, P., Klevansky, A., 2010. Classification of benign and malignant patterns in digital mammograms for the diagnosis of breast cancer. Expert systems with applications 37, 3344-3351.

Vieira, S., Sousa, J., Runkler, T.A., 2009. Multi-criteria ant feature selection using fuzzy classifiers. Swarm Intelligence for Multi-objective Problems in Data Mining 242, 19-36.

Wang, Y.-M., Yang, J.-B., Xu, D.-L., 2006. Environmental impact assessment using the evidential reasoning approach. European Journal of Operational Research 174, 1885-1913.

Wei, L., Yang, Y., Nishikawa, R.M., Jiang, Y., 2005. A study on several machine-learning methods for classification of malignant and benign clustered microcalcifications. IEEE transactions on medical imaging 24, 371-380.

Xue, B., Zhang, M., Browne, W.N., 2013. Particle swarm optimization for feature selection in classification: A multi-objective approach. IEEE transactions on cybernetics 43, 1656-1671.

Xue, B., Zhang, M., Browne, W.N., Yao, X., 2016. A survey on evolutionary computation approaches to feature selection. IEEE Transactions on Evolutionary Computation 20, 606-626.

Yang, J.-B., 2001. Rule and utility based evidential reasoning approach for multiattribute decision analysis under uncertainties. European Journal of Operational Research 131, 31-61.

Yang, J.-B., Singh, M.G., 1994. An evidential reasoning approach for multiple-attribute decision making with uncertainty. IEEE Transactions on systems, Man, and Cybernetics 24, 1-18.

Yang, J.-B., Xu, D.-L., 2002. On the evidential reasoning algorithm for multiple attribute decision analysis under uncertainty. Systems, Man and Cybernetics, Part A: Systems and Humans, IEEE Transactions on 32, 289-304.

Zhang, Y., Xia, C., Gong, D., Sun, X., 2014. Multi-objective PSO algorithm for feature selection problems with unreliable data, International Conference in Swarm Intelligence. Springer, pp. 386-393.

Zhao, H., 2007. A multi-objective genetic programming approach to developing Pareto optimal decision trees. Decision Support Systems 43, 809-826.

Zhou, Z.-G., Liu, F., Jiao, L.-C., Wang, Z.-L., Zhang, X.-P., Wang, X.-D., Luo, X.-Z., 2013. An evidential reasoning based model for diagnosis of lymph node metastasis in gastric cancer. BMC medical informatics and decision making 13, 123.

Zhou, Z., Folkert, M., Iyengar, P., Westover, K., Zhang, Y., Choy, H., Timmerman, R., Jiang, S., Wang, J., 2017. Multi-objective radiomics model for predicting distant failure in lung SBRT. Physics in Medicine and Biology 62, 4460.

Zio, E., Bazzo, R., 2012. A comparison of methods for selecting preferred solutions in multiobjective decision making. Computational intelligence systems in industrial engineering, 23-43.

